Revista de Ciencias Tecnológicas (RECIT). Universidad Autónoma de Baja California ISSN 2594-1925
Volumen 9 (3): e473. Julio-Septiembre, 2026. https://doi.org/10.37636/recit.v9n3e473

Review article

Photoacoustic techniques for non-destructive testing and evaluation: a comprehensive review

Técnicas fotoacústicas para ensayos y evaluación no destructiva: una revisión exhaustiva

José Mario Derramadero-Domínguez[1], Lenin Francisco Escamilla-Herrera[2], Orlando Miguel Medina-Cazares[3], Salvador Manuel Malagón-Soldara[1], Gerardo Gutiérrez-Juárez[2], Francisco Javier García-Rodríguez[1]

[1]Tecnológico Nacional de México / Instituto Tecnológico de Celaya. Av. Antonio García Cubas 600, Celaya, Guanajuato 38010, México.
[2]División de Ciencias e Ingeniería, Universidad de Guanajuato Campus León. A.P. E-143, León, Guanajuato CP 37150, México.
[3]Tecnológico de Monterrey, Escuela de Ingeniería y Ciencias, Blvd. Enrique Mazón López 965, 83000, Hermosillo, Sonora, Mexico.

Autor de correspondencia: Francisco Javier García-Rodríguez, Tecnológico Nacional de México / Instituto Tecnológico de Celaya. Av. Antonio García Cubas 600, Celaya, Guanajuato 38010, México. E-mail: francisco.garcia@itcelaya.edu.mx. ORCID: 0009-0003-1816-4070.

Received: April 15, 2026 **Accepted:** July 11, 2026 **Published:** August 26, 2026

Abstract. - *Non-Destructive Testing (NDT) is critical for industrial safety, yet traditional methods face limitations regarding coupling requirements and complex materials. This work presents a systematic review of photoacoustic technology as an advanced alternative, combining optical penetration with ultrasonic advantages to enable non-contact, high-resolution inspections. The study analyzes its successful application across metals, batteries and semiconductors for multiscale defect detection. Results confirm that photoacoustics is a consolidated tool that promises to evolve from simple defect detection to predictive lifespan analysis in advanced manufacturing. This review was conducted through a structured bibliographic search in Scopus, Web of Science, and IEEE Xplore, covering English-language publications from 2020 onward, with selection criteria focused on photoacoustic techniques applied specifically to engineering and industrial NDT/E, excluding biomedical in vivo studies.*

Keywords: Photoacoustic; Internal defects; Non-destructive testing.

Resumen. - *Las Pruebas No Destructivas (NDT) son fundamentales para la seguridad industrial, sin embargo, los métodos tradicionales presentan limitaciones relacionadas con los requisitos de acoplamiento y los materiales complejos. Este trabajo presenta una revisión sistemática de la tecnología fotoacústica como una alternativa avanzada, que combina la penetración óptica con las ventajas ultrasónicas para habilitar inspecciones sin contacto y de alta resolución. El estudio analiza su aplicación exitosa en metales, baterías y semiconductores para la detección multiescala de defectos. Los resultados confirman que la fotoacústica es una herramienta consolidada que promete evolucionar desde la simple detección de defectos hacia el análisis predictivo de vida útil en la manufactura avanzada. El análisis se realizó mediante una búsqueda bibliográfica estructurada en Scopus, Web of Science e IEEE Xplore, considerando publicaciones en inglés desde 2020 hasta la fecha. Los criterios de selección se centraron en técnicas fotoacústicas aplicadas específicamente a ensayos y evaluación no destructiva en contextos industriales y de ingeniería, excluyendo estudios biomédicos in vivo.*

Palabras clave: Fotoacústica; Defectos internos; Evaluación no destructiva.

1. Introduction

Leading technology industries rigorously validate new components, but certain characterization methods, such as those estimating Young's modulus or Vickers hardness, are inherently destructive and compromise the integrity of the sample. In contexts where structural integrity is prioritized, such as detecting manufacturing defects, assessing material fatigue, or monitoring motor shafts after operation, destructive testing becomes prohibitive due to high costs or downtime. In response, Non-Destructive Testing (NDT) has been progressively implemented and employed across different industries. It encompasses a set of fundamental techniques to ensure the safety, reliability, and operability of various components without damage that alters their functionality.

Some examples of highly demanding technology industries include aerospace, civil infrastructure, automotive, and power generation, where the early detection of structural defects (subsuperficial imperfections, cracks, porosity, corrosion, or delamination) is not only a matter of quality control but a critical measure to prevent catastrophic failures and to optimize preventive maintenance cycles. Traditional NDT techniques have been effective for decades but exhibit limitations when facing the challenges of modern manufacturing, including the need for couplants and physical contact, radiological risks, and restrictions on conductive materials and surface defects [1- 4].

Currently, the most common techniques are electromagnetic methods, ultrasonic techniques, and liquid penetrant testing. For example, for conductive metals, the eddy current non-destructive testing is particularly useful because, unlike other electromagnetic methods, the material does not need to be ferromagnetic and allows crack detection by monitoring the changes in the eddy currents. One advantage is that it does not require direct contact between the sensor and the component under evaluation, but is limited to superficial inspection [5,6]. Another type of NDT requires the use of chemical reagents or specialized dyes, and while they are classified as non-destructive, these methods are considered invasive since they involve the application of external substances to the material, a process that relies on the capillarity phenomenon. On a clean and dry surface, the penetrant is applied by dipping, spraying, or brushing, then after a certain dwell time (depending on the dye), the excess penetrant is removed, a developer is applied, and surface cracks become visible to the inspector [7].

The conventional pulse-echo ultrasonic testing (UT) is generally applied using piezoelectric elements, which act as both emitter and receiver. The emitter generates high-frequency sound waves, and then the emitter becomes the receiver, detecting reflections that occur at interfaces, defects, or cracks within the material, by analyzing the position of these reflections, the defect can be located. Unfortunately, this method is limited to planar geometries, since accurate reflection analysis requires surfaces that are flat and perpendicular to the incident ultrasonic waves, since complex or curved geometries distort the propagation path, making defect localization unreliable [8,9]. Another example of NDT is radiographic testing (RT), which uses ionizing electromagnetic radiation that passes through the inspection sample and impinges on a sensitive medium, producing an image that reveals internal defects. However, the method has low sensitivity to defects aligned with the radiation path, and its effectiveness also depends on the relative size of the defect compared to the overall sample [10].

Chemical reagents, radiographic testing, or X-ray inspection may pose hazards to inspectors if the techniques are not applied appropriately, therefore requiring specialized personnel, a challenge that is further intensified by the incorporation of advanced materials, composites, and additive manufacturing

ISSN: 2594-1925

processes, making new methods indispensable. In recent years, the National Aeronautics and Space Administration (NASA) has been working on developing and implementing composite structures and addressing the respective certification challenges, with the aim of applying them in military and space fields. NASA reports that traditional NDT methods designed for isotropic materials, such as metals, are not always suitable for composite applications [11].

In recent decades, photoacoustic imaging (PAI) has emerged as a promising approach to overcome several limitations of conventional NDT techniques. By combining optical excitation with ultrasonic wave detection, PAI enables tunable resolution, subsurface sensitivity, and operation under different experimental conditions. These features make photoacoustic-based methods attractive for the inspection of complex industrial components, advanced materials, and manufacturing processes where contact, coupling media, or ionizing radiation may be undesirable.

The photoacoustic (PA) effect was first discovered by Alexander Graham Bell in 1880 and can be broadly described as the generation of acoustic waves following the absorption of modulated or pulsed electromagnetic radiation by a material [12]. In modern implementations, laser sources are commonly used to induce localized heating, which produces transient thermoelastic expansion and, consequently, the generation of acoustic pressure waves in the frequency range of ultrasound. In solids, this process can generate different wave modes, including longitudinal, transverse, Rayleigh, and Lamb waves, depending on the optical excitation conditions, material properties, and sample geometry [13–15].

When pulsed lasers are employed to generate ultrasonic waves, the technique is commonly referred to as laser-induced ultrasound (LIUS). In NDT/E applications, LIUS and laser ultrasonic testing (LUT) are closely related but differ mainly in their detection strategy. In LIUS, acoustic signals are typically detected using contact sensors, commonly piezoelectric transducers coupled to the sample, whereas LUT generally relies on optical detection schemes such as interferometry or laser vibrometry. Therefore, LUT can operate in a fully non-contact configuration, making it particularly attractive for industrial scenarios involving rough surfaces, high temperatures, moving parts, or geometrically complex components [16,17].

The primary scientific objective of this comprehensive review is to critically evaluate and systematize recent methodological advancements in photoacoustic techniques, strictly applied to Non-Destructive Testing and Evaluation (NDT/E). To this end, this paper is organized into five sections, starting with the introduction that presents a general overview of NDT techniques, subsequently, the background section provides a formal (mathematical) framework of the PA effect. The next section presents the *search strategy and selection criteria* then outlines the systematic approach adopted for the bibliographic search and article selection. Subsequent sections present recent developments in PA technology-based NDT applied to metallic materials and in certain cases, to specific industrial sectors; finally, the paper concludes with a synthesis of the main findings and a discussion of future outlooks.

In contrast to many previous reviews that have primarily focused on biomedical photoacoustic imaging or on general laser ultrasonic methods [16,17,19], this review addresses a more specific and less extensively systematized domain: the use of photoacoustic-based techniques for non-destructive testing and evaluation (NDT/E) of engineering materials and industrial structures. The analysis emphasizes recent applications involving metallic structures, battery materials and systems, additive manufacturing components, semiconductor materials, and other technologically relevant inspection scenarios. The main contribution of this work lies in establishing a comparative framework for CW-modulated PA, pulsed PAI, PACT,

ISSN: 2594-1925

PAM, and LUT, highlighting their operational trade-offs in terms of contact requirements, defect scale, penetration depth, spatial resolution, signal acquisition strategy, and industrial scalability.

2. Background

Techniques based on the PA effect have already been described in the literature, and a physical model based in two coupled differential equations is widely accepted to describe this phenomenon. Equation (1) represents the heat diffusion equation for the temperature field T (r, t) which is coupled with the Equation (2) for the acoustic pressure field, P (r, t) [18,19].

$$\left(\frac{\partial}{\partial t} - \chi\, \nabla^2\right) T(r,t) = \frac{1}{\rho C_p}\left[H(r,t) + T_0 \beta\, \frac{\partial}{\partial t} P(r,t)\right]; \tag{1}$$

$$\left(\frac{\partial^2}{\partial t^2} - c^2\, \nabla^2\right) P(r,t) = \rho_0 \beta\, \frac{\partial^2}{\partial t^2} T(r,t). \tag{2}$$

Where $\chi \equiv \kappa / \rho_0 CP$ is the thermal diffusivity, κ is the thermal conductivity, ρ_0 and T_0 are the unaltered mass density and temperature, respectively, CP is the heat capacity at constant pressure, and β is the thermal coefficient of volume expansion. This classic model is widely referenced in literature and regarded as the cornerstone of the PA effect. To calculate the exact solutions to this system of differential equations, the literature usually employs two approximations. The first one is the *stress confinement* (SC), which occurs when the acoustic relaxation time defined as the time required by the sample to expand over the illuminated region, is larger than the laser pulse duration. In this case, while laser illumination heats the sample, the volumetric expansion of the sample is negligible. The second condition is thermal confinement (TC) which implies that heat diffusion is negligible, meaning that the thermal relaxation time is much longer than the laser pulse duration [20,21].

Before fully addressing the solution of the fundamental photoacoustic equations, an approximate image can often be obtained directly from the experimental signals, providing a practical reconstruction without initially relying on complex theoretical models. Figure 1 illustrates the different scanning modes commonly employed in PAI. Figure 1(a) presents the experimental arrangement, which serves as the basis for the subsequent acquisition schemes. The first mode is the Amplitude Scan (A-scan), which produces a single signal from the sample, as shows Figure 1(b), allowing a rapid examination but provides limited information typically just the time and amplitude of the signal. The next mode is the Brightness Scan (B-scan) (Figure 1 (c)), which is a compilation of A-scans that yield a 2D image [22]. Based on B-scans, different models can be used to reconstruct images from acoustic signals, the most common being Delay-and-Sum (DAS) [23,24]. Finally, the Constant-Depth / Plan Scan (C-scan) (Figure 1 (d)), which is a compilation of B-scans, enables a three-dimensional reconstruction of the sample, revealing the exact position of any detected defect [22].

ISSN: 2594-1925

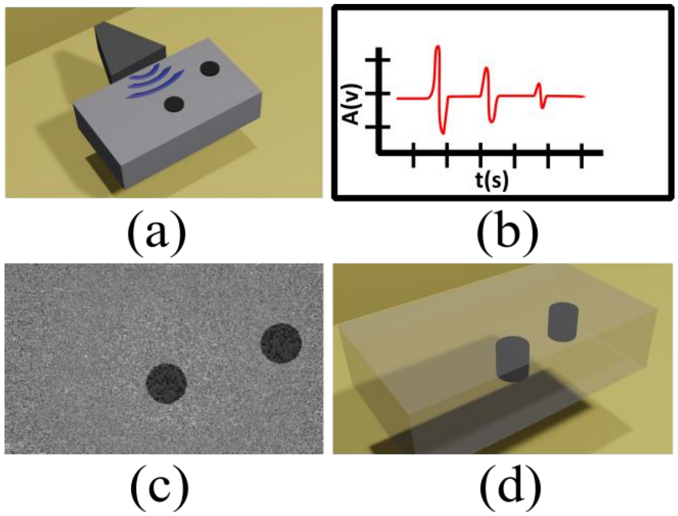

Figure 1. Illustrative example of an ultrasound transducer experimental arrangement (a). Emulated signal obtained by an A-scan (b). Emulated image formed by a B-scan (c). Typical image formed by a C-scan (d).

In general, techniques based on the photoacoustic (PA) effect can be broadly classified into two major groups, modulated photoacoustic and pulsed photoacoustic (PPA). The modulated photoacoustic approach is often described in literature as photoacoustic excitation using a continuous-wave (CW) laser [25], as illustrated in Figure 2 (a). In this configuration, the most common experimental arrangement involves the use of a mechanical chopper to modulate the CW laser and generate pulses [26], or alternatively, a function generator may be employed. For the PPA there are lasers capable of producing ultrashort pulses, typically in the nanosecond or even picosecond range. In both cases, the selection of parameters depends on the specific application, typically varying the wavelength, modulation frequency, energy per pulse, and pulse duration.

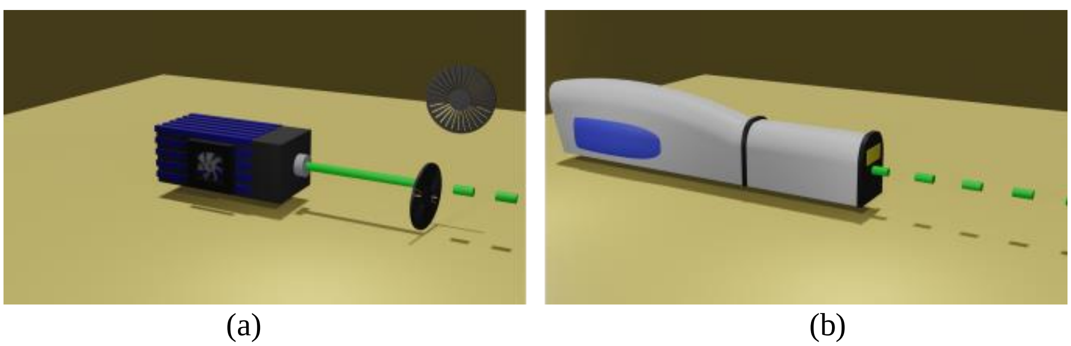

Figure 2. (a)Continuous laser with a mechanical chopper. (b) Pulsed laser.

PPA techniques have gained increasing relevance in recent years not only in NDT applications, hence in this work, some PPA methods are presented, modulated photoacoustic**,** principles of PAI, photoacoustic tomography (PACT), photoacoustic microscopy (PAM) and laser ultrasonics (LUT). Photoacoustic microscopy itself is subdivided into two approaches, optical-resolution photoacoustic microscopy (OR-PAM), where the resolution limit is determined by the optical focus, and acoustic-resolution photoacoustic microscopy (AR-PAM), where the resolution limit is dictated by the focus of the ultrasound transducer.

ISSN: 2594-1925

3. Search Strategy and Selection Criteria

To ensure a systematic and rigorous collection of the most recent literature, a structured search strategy was implemented based on the five main thematic axes of this review. Bibliographic queries were conducted between February 2 and March 21, 2026, using the Scopus, Web of Science, and IEEE Xplore databases. In order to guarantee the currency of the state of the art, the publication window was strictly limited to works published from 2020 onwards and only those written in English.

Table 1. Inclusion and exclusion criteria used for bibliographic selection.

Criterion	Inclusion	Exclusion
Publication period	Works published from 2020 onward	Works published before 2020, except historical or contextual references
Language	English-language publications	Non-English publications
Application field	Engineering materials, industrial structures, and NDT/E applications	Biomedical, clinical, or in vivo biological tissue studies
Technique	PA, PAI, PACT, PAM, LIUS, and LUT	Non-photoacoustic or unrelated optical/acoustic techniques
Contribution type	Experimental, theoretical, numerical, or methodological studies relevant to NDT/E	Papers without direct relevance to NDT/E or already extensively covered in previous reviews

The search was carried out independently for each of the five central topics, with specific search equations formulated through the use of Boolean operators and adapted keywords to capture the most representative contributions in each technological area. Examples of these combinations include [LIU AND modulated laser] and [photoacoustic AND continuous laser]. The initial selection process consisted of screening articles by reading titles and abstracts, prioritizing original research that allowed for the comparison of methodologies and results.

For four of the five thematic axes, the selection intentionally focused on works presenting both theoretical developments and their corresponding experimental validation. For the fifth axis, the selection deliberately emphasized studies with theoretical contributions and numerical simulations, aiming to deepen the modeling foundations of the topic. To ensure the novelty of this review, primary articles already thoroughly analyzed in existing review papers were excluded, thereby avoiding redundancy in the literature.

Finally, a strict exclusion criterion was applied based on the definition of Non-Destructive Testing and Evaluation (NDT/E). Since the scope of NDT/E is limited to the inspection of materials and structures in engineering and industrial contexts, studies focused on biomedical, clinical, or in vivo biological tissue applications were excluded. Medical literature was retained only for brief historical and conceptual references when necessary to provide context.

ISSN: 2594-1925

4. Applications

4.1 Modulated Photoacoustic based on CW laser.

With the advancement of semiconductor technology, continuous wave (CW) laser diodes have emerged as a promising alternative, potentially capable of replacing the currently used pulsed lasers in the future. This technology offers significant advantages, including lower cost, reduced size, and improved portability compared with convencional Nd:YAG laser systems [27].

However, several challenges remain, for instance, the fluence of most commercial diodes is significantly lower than pulsed lasers, and precise control is required to ensure uniformity in the generated pulses. Their limited power directly impacts the signal-to-noise ratio (SNR), since the diode emission is the single source of the photoacoustic effect. A lower fluence reduces optical absorption, which is one of the principal parameters determining the amplitude of the resulting signal. A second limiting factor is the intrinsic sensitivity of the sensor, and finally, the separation distance between the optical source and the sensor also plays a critical role [28].

To address the issue of low SNR when measuring at long distances from the source, Vangi *et al.* [29] developed a new method to increase the signal amplitude based on constructive interference between elastic waves. They first evaluated the signal at a considerable distance from the source and then, to demonstrate the performance of this technique, applied it to the identification of an elliptical crack on a rail. Figure 3 shows the considered experimental setup. Position 1 is located 0.1 m from the source, whereas position 2 is 1.3 m from the source. The latter distance was used to demonstrate that constructive interference could reach the sensor. The figure also shows the laser diode power, the use of an amplifier, and the oscilloscope employed to collect the resulting data.

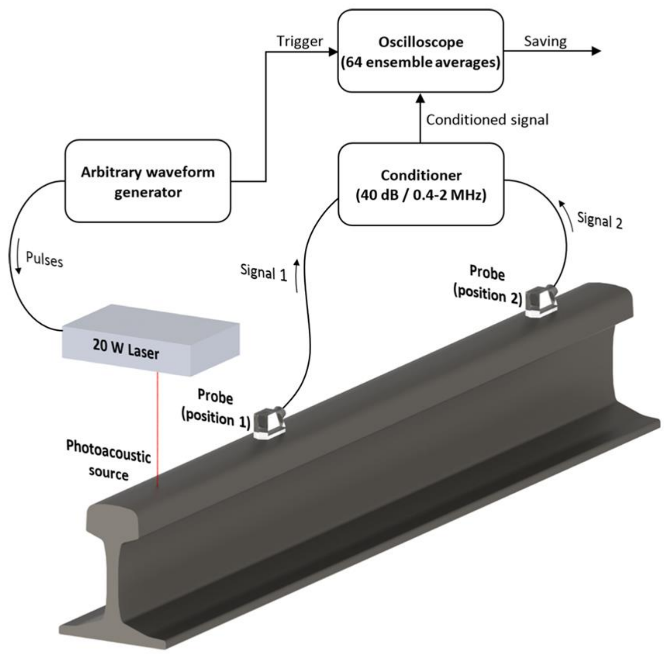

Figure 3. Experimental arrangement on a rail for constructive interference enhancement. Image taken from Vangi et al [29].

ISSN: 2594-1925

To achieve constructive interference, the control of the laser diode was implemented through Transistor-Transistor Logic (TTL), which allows modulation of the *on* time of the square input signal, as well as the *off* time and the interval between repetitions. Moreover, achieving interference in the time domain has shown that the number of pulses is related to modifications in the central frequency spectrum, particularly when the pulse count is high, this finding provides the opportunity to design and optimize the experimental arrangement for dedicated applications.

To validate the proposed methodology, a defect was intentionally fabricated between both positions, measuring 12 mm in width and 2.5 mm in depth, both the sensor and the laser were displaced along the x-direction of the rail, as shown in Figure 4(a). Figure 4(b) presents the resulting B-scan, where the crack area is highlighted, beyond obtaining the crack width, since crack depth is a function of the x-coordinate, the influence of different crack depths on the acquired signal can be evaluated. This variation clearly modifies the amplitude of the acquired ultrasound, and the SNR can be analyzed to estimate the crack depth by comparing it with the SNR of a sample without cracks. For a 1 mm deep defect, this relation decreases by almost 2 dB, while for a 2.5 mm deep crack the relation drops to less than half of its initial value.

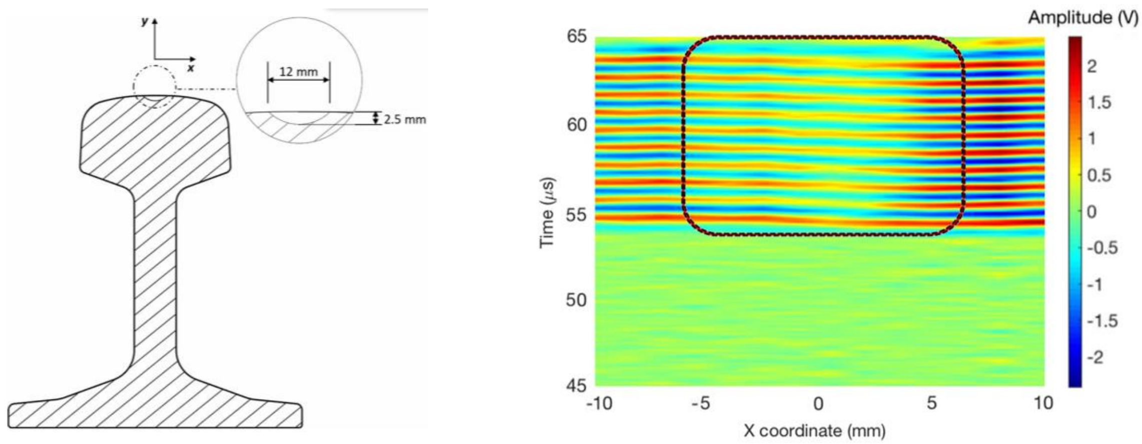

(a) (b)

Figure 4. (a)Definition of crack measurements. (b) B-scan obtained from the experiment as a function of time, distance and amplitude. Image taken from Vangi et al [29].

4.2 Principles of Pulsed Photoacoustic Imaging (PAI)

Although methodologies that solve the photoacoustic equations (inverse problem) are essential for full reconstruction, numerous studies demonstrate that high-resolution B-scan and C-scan images can be obtained directly from experimental signals but remain a partial representation rather than a complete reconstruction [30]. The B-scan method has been widely applied in the biomedical field due to its high resolution in the morphological characterization of tissues in both animal and human studies [31]. More recently, similar strategies have been extended to the area of non-destructive testing (NDT), particularly in metals, where the technique enables high accuracy in experimental measurements.

ISSN: 2594-1925

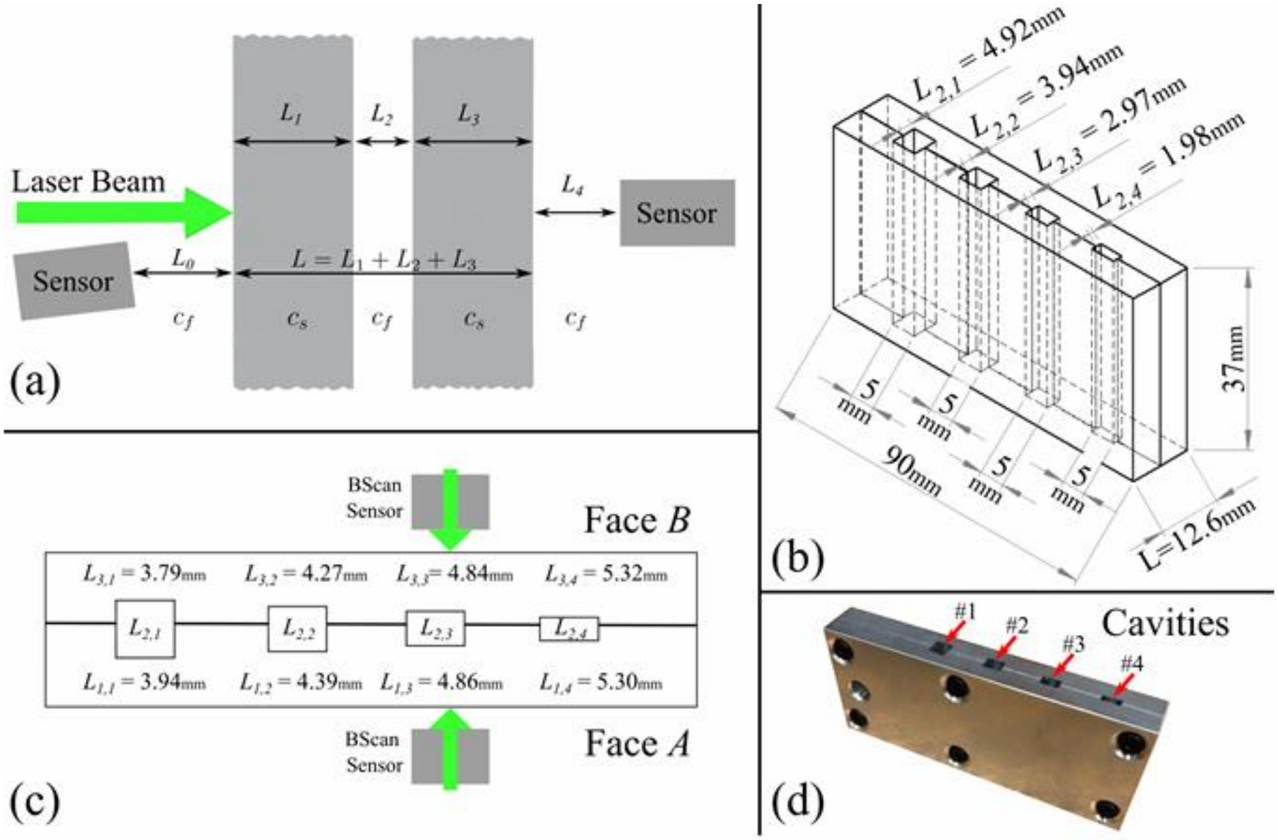

Figure 5. (a) Detailed schematic representation of the experimental configuration to determine the separation between two slabs. (b) Isometric drawing showing actual cavity dimensions, numerated from left to right. (c) Cross-section of the slab with the artificial cavities. (d) Picture of the slab with the artificial cavities. Image taken from Rojas et al [32].

Figure 5 shows the specimen used in an NDT study based on LIUS, which consisted of two aluminum slabs joined together, designed to create rectangular cavities between the plates in order to emulate holes or imperfections in a metallic material. In this study, Rojas et al. [32] propose an analysis of the experimental signals (A-scan), based on the time-of-flight (TOF) method. From these A-scans, information regarding the thickness of the sample can be obtained through the TOF, which corresponds to the interval between the first pulse observed in the experimental data and the subsequent reflection. In a homogeneous sample, the TOF remains constant; therefore, variations in TOF indicate the presence of a discontinuity, such as a hole. The TOF is defined as $\tau = 2L/c$, where L and c represent the thickness and the sound speed of the sample, respectively.

The sample contained four cavities with different dimensions, and the authors focused their evaluation on the third cavity. Both sides of the plate were examined independently through B-scan acquisition. To compare the experimental results, the sample dimensions were measured using a vernier caliper, the cavity dimensions were 12.6 mm × 90.0 mm × 37.0 mm, as shown in Figure 5. Additionally, two equations were derived to relate the TOF to the sample size.

ISSN: 2594-1925

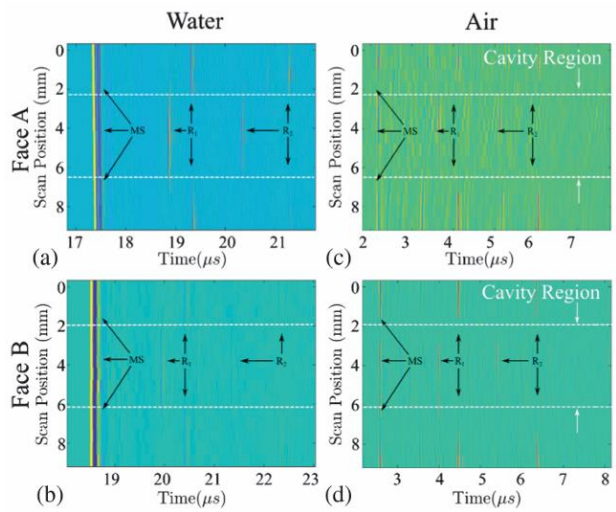

Figure 6. B-scan generated from the raw LIU signals for both faces in different media. Image taken from Rojas et al [32].

To achieve a more realistic evaluation, two experimental conditions were considered: a controlled laboratory setup using a water tank, and an air-based configuration where coupling was provided through gel. For each configuration, two B-scans were performed, Figure 6 presents the B-scans obtained from each face of the plate; subsequently Figure 7 illustrates the combination of the two sides together with the measurements derived from the proposed equations. The authors found a minimal variation between 0.41% and 5.72% (20–230 µm) in the measurements performed in water, and between 0.86% and 6.46% (20–220 µm) in those performed in air. Moreover, the results demonstrate that it is possible to measure the distance between the two slabs (kissing bond), which was approximately 49 µm in water and 29 µm in air.

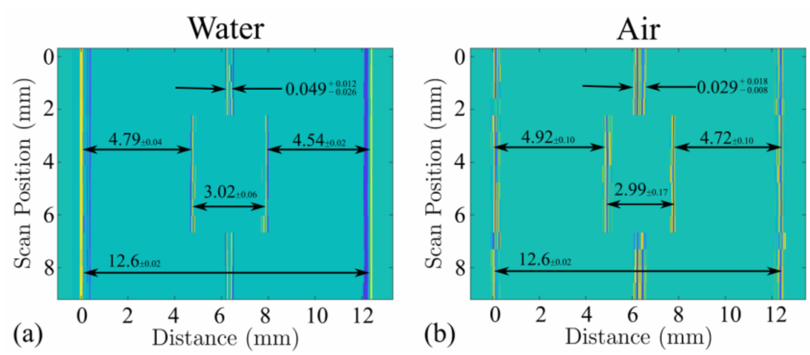

Figure 7. Reconstructed images generated from the combination of faces A and B shown in Figure 6. Image taken from Rojas et al [32].

4.3 Photoacoustic tomography (PACT)

Photoacoustic computed tomography (PACT) differs fundamentally from other photoacoustic techniques in its acquisition mode and its ability to achieve deeper penetration into biological samples. Its primary objective has traditionally been the investigation of deep tissues, particularly in applications such as vascular imaging, tumor detection, and implant monitoring. Similar to other branches of photoacoustic, PACT has subsequently been adapted to NDT. Several methodologies have been developed to acquire

ISSN: 2594-1925

data using this technique. The most common approach involves a circular arrangement of sensors, enabling parallel acquisition in which information from all detectors is collected simultaneously. An alternative method employs a single sensor aligned with the laser, combined with rotation of the sample to obtain multiple projections [33- 35].

Nevertheless, both methodologies allow the creation of B-scan images directly from experimental data, while solving the inverse problem could provide all that is needed for a complete image reconstruction. Yet this does not always occur, since methods based on the inverse problem may introduce artifacts or reduce contrast in the final image. To address this issue, dual illumination has been applied to metallic cylinders, in their work, Moock *et al* [36] developed this methodology for the characterization of material properties and compared the results with a simulation framework using the PATLAB toolbox.

Figure 8 shows the experimental arrangement of the dual illumination technique, which involves two pulsed lasers, consequently, two transducers were also used. The study was conducted in water, which served as the coupling medium. Five different metallic cylinders were used as specimens (aluminum, brass, bronze, copper, and stainless steel), each with an inner diameter of 4 ± 0.01 mm and an outer diameter of 24.91 ± 0.12 mm. For each specimen, the sound speed was determined experimentally. Additionally, the detector positions were labeled as “north” (N), “east” (E), “south” (S), and “west” (W).

The signal obtained from this dual illumination setup presents the challenge that the direction of signal propagation is not inherently linked to spatial coordinates. Therefore, a mathematical transformation was employed, in which a forward signal, denoted as g, is interpreted in the backward direction. This process involves generating a mirrored time sequence, denoted as g', which is then registered within the same temporal frame as the opposing signal. By aligning these two sequences, the system can effectively synchronize the data acquired from different points of the circular array. This synchronization is achieved through the Hadamard product ($g \odot g'$), which is defined as the element-wise multiplication of two vectors or matrices of the same dimensions. This operation emphasizes points of intersection and coincidence between sensors, thereby reducing noise and isolating the relevant acoustic data, by applying this technique to various combinations of detector positions, all possible spatial interactions within the array can be evaluated.

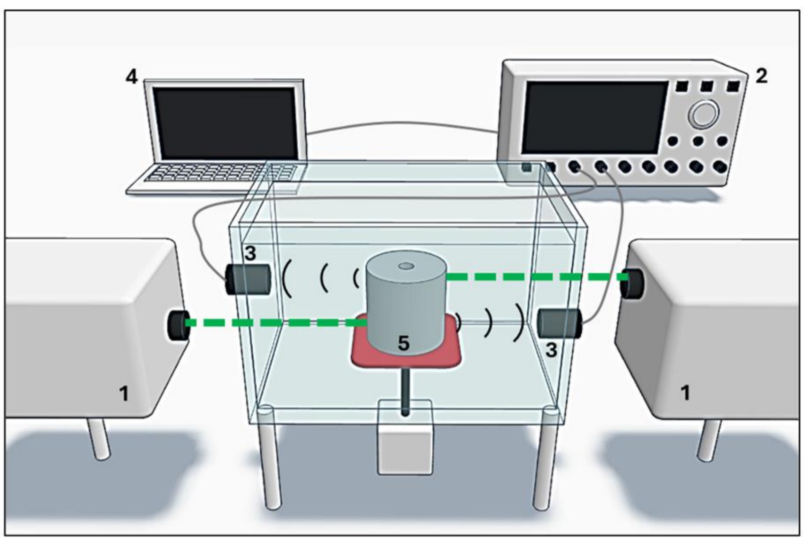

Figure 8. Schematic of the experimental setup, Image taken from Moock et al [36].

ISSN: 2594-1925

As a result of the experimental arrangement, Figure 9 depicts two images reconstructed by following the described methodology and employing the Delay-and-Sum (DAS) algorithm, the single-laser scan (left) exhibits pronounced artifacts, whereas the dual-illumination approach (right) demonstrates superior performance by mitigating such artifacts. Nonetheless, further signal enhancement is required to resolve the internal structure of the hollow cylinder. A detailed analysis is presented in the referenced study with the aim of quantifying this similarity, the results confirm that dual processing effectively reduces randomness and uncertainty, thereby producing a cleaner image [36].

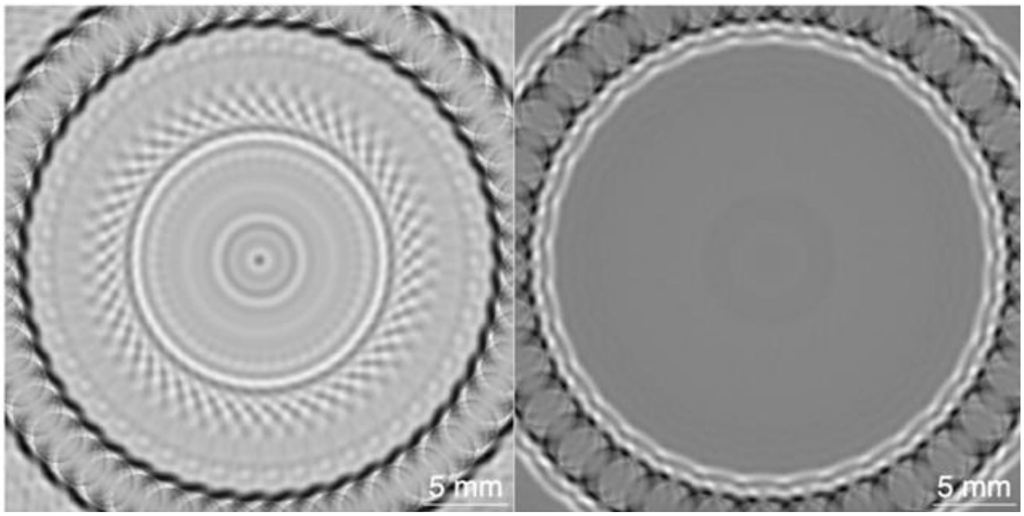

Figure 9. Primal (left) and dual (right) DAS reconstruction of the bronze cylinder, Image taken from Moock et al [36].

4.4 Photoacoustic Microscopy (PAM)

As portable technologies and battery-based energy storage systems have proliferated, new challenges have emerged, particularly in the electric vehicle industry, since their batteries face demanding conditions such as excessive temperatures and repeated charge-discharge cycles, these conditions can limit or reduce battery longevity [37].

In Figure 10, the fundamental structure of batteries is shown, which consists of two electrodes in contact with an electrolyte solution, these devices store electrical energy by the conversion of chemical energy through redox reactions at the anode and cathode [38]. New types of batteries have been investigated to address current challenges, these developments are based on various modifications, such as lithium-metal batteries, in which the typical graphite anode is replaced with a more energy-dense lithium metal to enhance energy storage. Nevertheless, microstructural failure mechanisms have generally been observed, known in literature as dendrites, which arise from inhomogeneous deposition and stripping of electrode metal during charge and discharge cycles, respectively [39,40]. Several NDT techniques can be used to assess dendrite growth, such as scanning and transmission electron microscopy, but these require sample preparation, making them unsuitable for rapid in situ observation, other techniques, such as X-ray microscopy, are unsuitable because lithium has a low electron density [41].

ISSN: 2594-1925

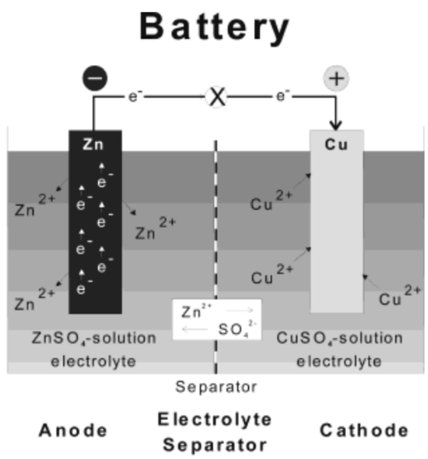

Figure 10. Fundamental battery composition. Image taken from Winter & Brodd [38].

Therefore, PAM was analyzed as a potential substitute for conventional NDT methods in batteries. *Liu et al* [41] constructed a Li/Li symmetric cell with a liquid electrolyte, as depicted in Figure 11(a). The Li electrodes exhibited a thickness of approximately 240 µm, while the electrolyte layer measured about 2 mm. To facilitate the experiment, one side of the cell was cut to obtain a flat sidewall (Figure 11(b)). Subsequently, the cell was sealed within a stainless-steel coin cell case for the charging process (Figure 11(c)). Figure 11(d) illustrates the Li/Li cell before and after charging, where the current direction dictates whether Li is stripped from or plated onto a given electrode. Finally, Figure 11(e) presents the cell voltage as a function of elapsed time under five distinct charging current densities.

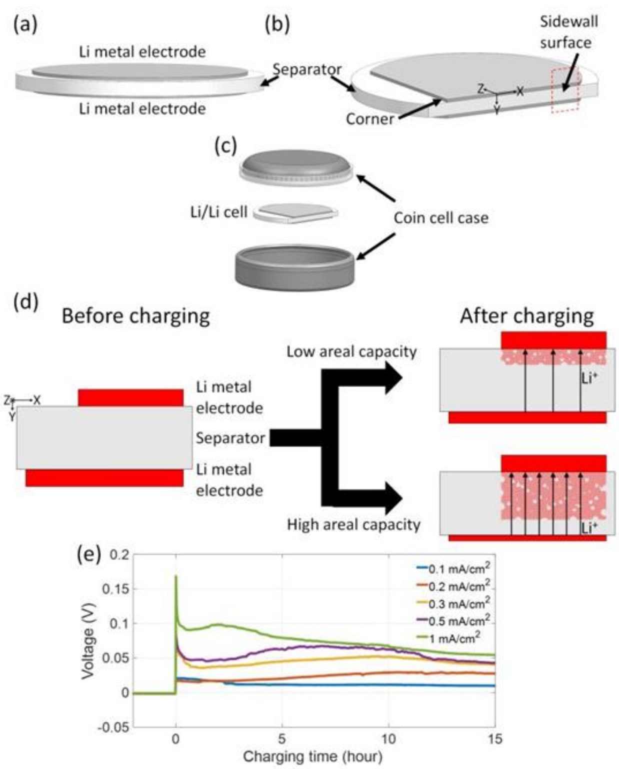

Figure 11. Li/Li cell used as a sample for dendrite growth. Image taken from Liu et al [41].

ISSN: 2594-1925

After the charging process, the stainless-steel coin cell case was removed, and the cell was sealed in a plastic bag filled with liquid to facilitate ultrasound coupling. In order to establish a comparison between conventional techniques and PAM, an Optical Microscopy (OM) method was employed. Figure 12(a) shows the sample holder, which contains markers on the top surface to aid in the comparison. Figures 12(b) and 12(c) highlight the contrast, which is more pronounced in the PAM image than in the OM image. Figures 12(d) and 12(e) illustrate the depth of focus (DOF) achieved by both methods; once again, PAM provides a superior DOF. These results reinforce the earlier observation that OM cannot directly visualize dendrite growth and offers limited depth information. Finally, Figure 12(b) presents a complete three-dimensional model reconstructed using PAM.

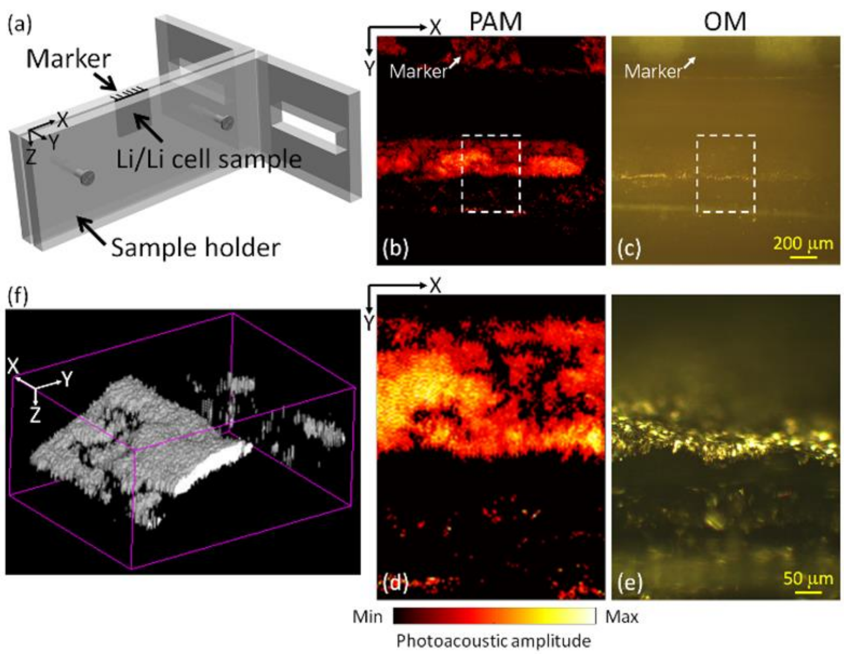

Figure 12. Li/Li cell analyzed by PAM and OM for dendrite growth. Image taken from Liu et al [41].

The cell configuration also enables the analysis of the electrolyte layer, which was fabricated using a GFS. This analysis revealed that Li protrusions were deposited in an inhomogeneous pattern and progressively increased as the charging current density was raised. It was found that PAM could penetrate up to ∼160 µm inside the GFS, whereas OM achieved a penetration depth of only ∼50 µm. This experimental evidence positions PAM as a potential tool for the study of dendrites. Future research could extend this approach to other types of battery cells, such as those employing sodium, magnesium, or zinc electrodes, which, based on the present results, appear technically feasible [41].

4.5 Laser ultrasonic (LUT)

In laser ultrasonic testing (LUT), a pulsed laser is used to induce the PA effect within the thermoelastic regime, thereby avoiding phenomena such as photodamage. Unlike other PPA techniques that used piezoelectric sensors, LUT commonly employs vibrometers or even interferometric detection schemes have been reported, such as a Fabry–Perot interferometer built with a continuous laser[42,43]. LUT has been investigated in several industrial applications, for instance, it has been applied to detect inter and

ISSN: 2594-1925

intralayer defects in additive manufacturing [44,45], in other cases, Finite Element Method (FEM) simulations have been conducted to study its application in aero-engine blades, where surface fatigue cracks frequently occur. Numerical results demonstrate that the surface acoustic waves induced by pulsed lasers are highly sensitive to surface-breaking cracks [46] and LUT has also been applied to visualize and characterize hidden notches in aluminum plates, achieving high spatial resolution [47].

Similar to the electric vehicle industry, the semiconductor industry is constantly searching for new materials and methods to meet the demands of devices ranging from simple and inexpensive to highly advanced. One of the key characteristics that determines whether a material is suitable for semiconductor applications is its bandgap, defined as the energy difference (measured in electronvolts, eV) between the Valence Band where electrons are strongly bound to atoms and the Conduction Band where electrons are free to move and generate current [48, 49]. Silicon carbide (SiC) stands out among semiconductor materials due to its wide bandgap, which enables a broad range of potential applications, as well as its compatibility with complementary metal oxide semiconductor (CMOS) processes [50].

In the semiconductor industry, as in other manufacturing sectors, fabrication-related defects can be mitigated but not entirely eliminated, therefore it remains essential to ensure and verify the absence of microcracks, internal defects, and other flaws that could limit the useful life or compromise the functionality of the material. Several techniques are employed to identify internal defects, such as the potassium hydroxide (KOH) corrosion method, a traditional chemical approach used to reveal defects in silicon carbide (SiC) crystals. This method, however, is destructive, as the dissolution process irreparably damages the sample. Moreover, available techniques for detecting surface or subsurface defects are often costly or require lengthy evaluation times [51,52].

As part of an exploratory investigation to implement LUT for the analysis of defects in SiC, Yin et al. [53] proposed a numerical study to clarify the relationship between defect parameters and acoustic vibrations. To this end, they developed a two-dimensional model in which the heat conduction equation is presented in Equation (3). In this formulation q represents the external heat source, K is the thermal conductivity, T is the temperature field as a function of time, ρ is the material density, and c is the specific heat capacity per unit volume.

$$\left(\frac{\partial^2 T(x,y,t)}{\partial x^2} + \frac{\partial^2 T(x,y,t)}{\partial y^2}\right) - \frac{\rho c}{K}\frac{\partial T(x,y,t)}{\partial t} = -\frac{q}{K} \quad (3)$$

Equation (4) describes how the acoustic vibration displacement depends solely on the material parameters and the temperature field [54]. λ is the first-order Lamé constant of the isotropic solid, u is the second-order Lamé constant, U is the displacement vector, and α is the coefficient of thermal expansion.

$$(\lambda + 2u)\nabla(\nabla \cdot U) - u\nabla^2 U - \alpha(3\lambda + 2\mathrm{u})\frac{\partial T(x,y,t)}{\partial t} = \rho\frac{\partial^2 T\boldsymbol{U}}{\partial t^2} \quad (4)$$

To apply the two-dimensional model developed, Figure 13 presents two configurations designed to study the interaction of acoustic waves with surface and internal defects. For the superficial defect, the sample has a width of 10 mm and a height of 5 mm, with a defect size of 0.1 × 0.05 mm. In the internal case, the defect is modeled 0.05 mm below the surface, and the excitation point is positioned at (−2, 0).

ISSN: 2594-1925

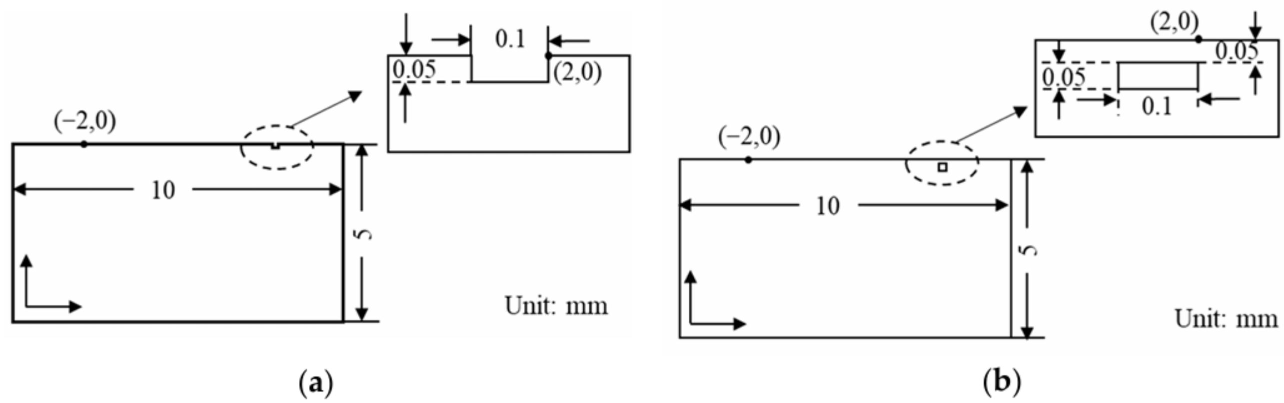

Figure 13. Schematic diagram of a specimen with a surface defect (a) or an internal defect (b). Image taken from Yin et al [53].

Through the analysis of numerical simulations, it is observed that the temperature at the excitation point depends on the repetition rate of the laser, which can be adjusted to ensure the maximum surface temperature of the material. Figure 14 shows the acoustic field distribution in SiC with a surface defect, where the behavior of the different waves can be observed. The pressure wave (P) propagates most rapidly, followed by the shear wave (S), while the Rayleigh wave (R) travels along the horizontal surface at a direction angle of 0°, the propagation angle of the pressure wave is greater than that of the shear wave.

Figure 14(a) shows that when the P-wave reaches the defect, part of the wave is reflected (rP) while another portion is transmitted through the defect (tP). Subsequently, some of the P-wave energy is converted into a shear wave (PS) and a Rayleigh wave (PR), as if the impact at the crack edge generates new wave modes. In Figure 14(b) the Rayleigh wave (R) carries the most energy and propagates along the surface. Upon encountering the micro-defect, a reflected Rayleigh wave (rR) is formed, while most of the R-wave energy is transmitted beneath the defect and continues its path (tR). Finally, a small fraction of the Rayleigh wave is also converted into shear waves (RS) and pressure waves (RP), which continue to propagate.

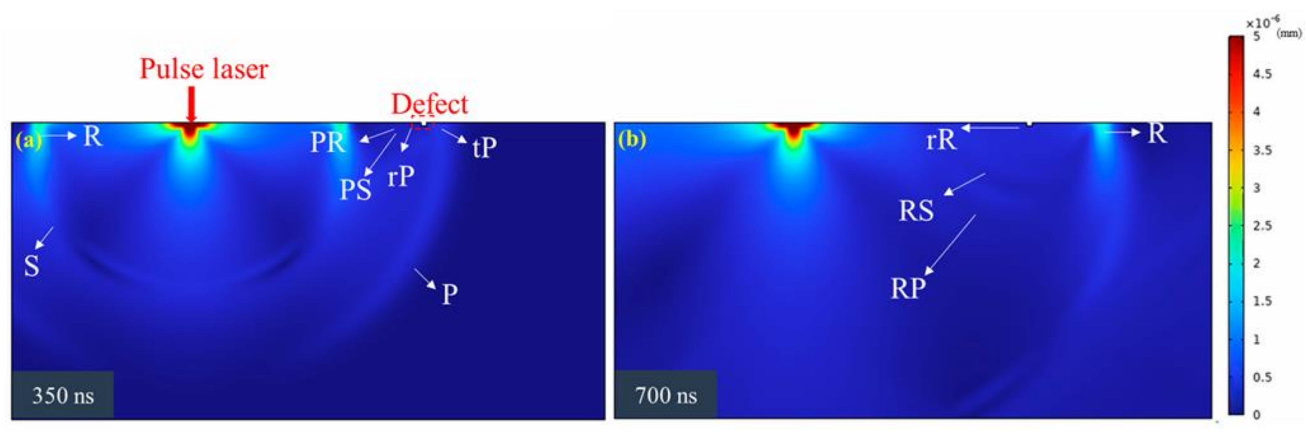

Figure 14. Acoustic field distribution of specimens with a surface defect at (a) t = 350 ns and (b) t = 700 ns. Image taken from Yin et al[53].

ISSN: 2594-1925

For the internal defect shown in Figure 15(a), most of the energy is transmitted (tR), flowing along both the upper and lower surfaces of the defect, a small portion of the wave strikes the defect edge and is reflected (rR). At the right corner of the defect, a mode transition occurs, generating a converted Rayleigh wave (RSR). Additionally Figure 15(b) illustrates that this mode transition is more pronounced than in the case of surface defects; here, the Rayleigh wave is partially converted into a shear wave (RS) and a pressure wave (RP). In conclusion, the simulation results indicate that surface defect edges can be identified by the abrupt increase in Rayleigh wave amplitude. However, when the defect depth exceeds the Rayleigh wavelength, reflection (rR) nearly disappears and the transmitted wave remains unaffected. In such cases, detection is only possible through pressure (P) and shear (S) waves, since the Rayleigh wave ceases to interact with the defect [53].

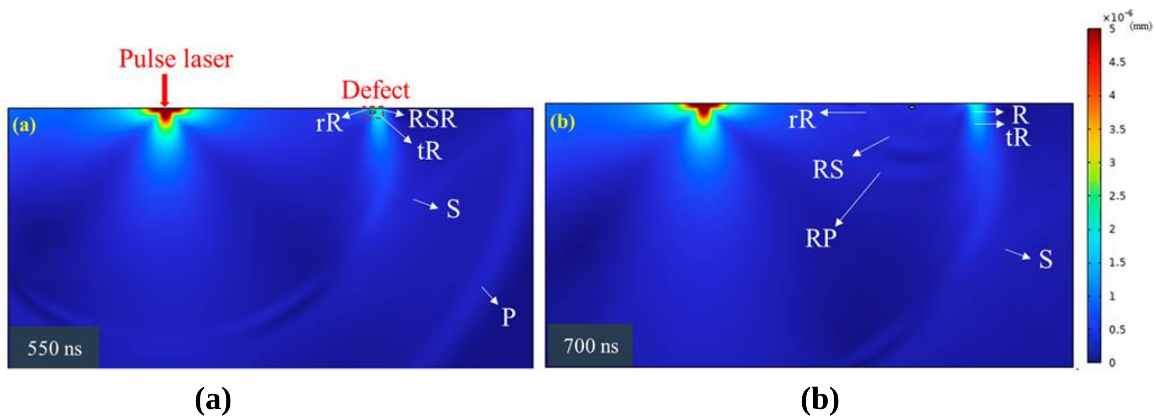

Figure 15. Acoustic pressure field at (a) t = 550 ns and (b) t = 700 ns of a specimen with an internal defect. Image taken from Yin et al [53].

4.6 Comparative synthesis of photoacoustic techniques for NDT/E

To synthesize the main findings discussed in the previous subsections, Table 2 presents a comparative overview of the photoacoustic-based techniques analyzed in this review. The comparison emphasizes the operational trade-offs among excitation source, detection strategy, contact requirements, defect scale, penetration capability, main advantages, limitations, and representative NDT/E applications. This synthesis highlights that no single technique is universally optimal; instead, the suitability of each approach depends on the inspection scenario, material characteristics, defect geometry, required spatial resolution, and industrial implementation constraints.

ISSN: 2594-1925

Table 2. Comparative overview of photoacoustic based techniques for NDT/E.

Technique	Excitation source	Detection strategy	Contact requirement	Typical defect scale	Penetration capability	Main advantages	Main limitations	Representative applications
CW-modulated PA	Modulated continuous-wave laser or laser diode	Piezoelectric sensor or optical detection	Often requires sensor coupling, depending on the configuration	Surface and near-surface defects	Low to moderate	Low cost, compact setup, potential portability	Lower SNR due to limited optical power; requires careful modulation control	Crack detection in rails and metallic components
Pulsed PAI / LIUS	Pulsed laser	Ultrasonic transducer; commonly piezoelectric detection	Usually requires acoustic coupling	Internal cavities, kissing bonds, subsurface discontinuities	Moderate	High accuracy for time-of-flight-based sizing; suitable for B-scan and C-scan inspection	Coupling requirements; image formation may remain partial without full reconstruction	Metallic plates, internal cavities, kissing bond evaluation
PACT	Pulsed laser	Sensor array or rotating detector configuration	Usually requires a coupling medium	Internal defects and volumetric discontinuities	Moderate to high	Tomographic reconstruction capability; useful for internal defect localization	Reconstruction artifacts; computational cost; expensive pulsed laser sources	Hollow metallic cylinders and internal structure inspection
PAM	Focused pulsed laser	Focused ultrasonic detection	Depends on the configuration; coupling is often required	Microdefects, dendrites, microscale discontinuities	Low	Very high spatial resolution; suitable for microstructural inspection	Limited penetration depth; slow scanning for large areas	Battery materials, dendrite growth, microscale inspection
LUT	Pulsed laser	Optical interferometry, laser vibrometry, or Fabry–Perot detection	Fully non-contact in typical configurations	Surface cracks, subsurface flaws, porosity, lack-of-fusion defects	Moderate	Suitable for harsh environments, complex geometries, moving parts, and materials where couplants are undesirable	Sensitive to surface roughness; higher system cost; signal processing requirements	Additive manufacturing, SiC inspection, CMCs, aerospace and energy components

ISSN: 2594-1925

As summarized in Table 2, CW-modulated PA offers the most accessible and potentially portable configuration, but its performance is commonly limited by SNR constraints. Pulsed PAI and LIUS provide accurate defect sizing through time-of-flight analysis, although they often require acoustic coupling. PACT extends the inspection capability toward tomographic reconstruction of internal structures, but at the cost of more demanding reconstruction algorithms and possible artifacts. PAM provides the highest spatial resolution among the techniques reviewed, making it suitable for microscale inspection, although its limited penetration depth restricts large-volume applications. In contrast, LUT offers the most favorable conditions for fully non-contact industrial inspection, particularly in scenarios involving complex geometries or materials where couplants are not acceptable.

5. Conclusions and Outlook

Overall, the different branches of PPA reveal, a clear technological difference between spatial resolution, penetration depth, and industrial viability. While techniques such as PAM and PACT address specific needs in micro-defect detection and volumetric reconstruction, their limitations in scalability and cost remain significant. In this context, for continuous and cost-effective monitoring, modulated PA employing CW lasers has been proposed as a highly accessible alternative that substantially reduces equipment costs [55]. Moreover, this continuous wave technology has been successfully integrated as an excitation source for the LUT technique [56], which has been distinguished as a robust methodology, offering remarkable versatility for inspections where conventional techniques fall; nevertheless, its effectiveness has been shown to depend strongly on the surface roughness of the analyzed material.

Despite these operational differences, the technical challenges associated with resolving complex internal structures are frequently shared across these disciplines. For instance, PACT methodologies applied to highly scattering and layered media, such as dental anatomy [57], have demonstrated that the implementation of targeted bandpass filtering can significantly optimize the acquired signal, resulting in a notable increase in lateral resolution [58]. In addition, the computational burden inherent in image generation has been effectively mitigated through the adoption of parallel computing techniques and finite element analysis methods (FEM) [59]. These advances in signal processing and computation, although initially validated in biological hard tissues, can be directly extrapolated to industrial Non-Destructive Testing (NDT), thereby accelerating and refining defect visualization.

In contrast, Laser Ultrasonic Testing (LUT) has consistently demonstrated a comparative advantage in real-world application where traditional contact methods are impractical. In the field of metal additive manufacturing, for example, LUT has proven highly effective in detecting complex defects such as lack of fusion between printed layers, micro-cracks, and internal porosities [60]. Similarly, in critical sectors such as aerospace and energy, the inspection of Ceramic Matrix Composites (CMCs) has posed a unique physical challenge. Owing to the inherent porosity of these materials, the liquid couplants required by conventional ultrasonic techniques would irreparably contaminate the sample; consequently, the fully non-contact nature of LUT has been regarded as a technically superior alternative [61]. To address its own limitations, recent investigations have focused on expanding the capabilities of LUT to achieve high-precision measurements even on rough or structurally imperfect surfaces [62].

Overall the photoacoustic effect possesses a wide range of applications, although it has achieved remarkable development in the biomedical field, its use for solving inspection problems in solid materials is becoming increasingly common. Much of its versatility lies in the ability to measure defects with high

ISSN: 2594-1925

precision, covering a scale that ranges from millimetric imperfections to micrometric discontinuities. While penetration depth in solids remains a challenge for certain applications, the photoacoustic technique clearly surpasses many conventional technologies that prove ineffective in the presence of sample porosity, require strictly non-contact inspections, or are limited exclusively to ferromagnetic materials.

The second major challenge for the widespread adoption of photoacoustic techniques is the high cost of traditional pulsed lasers. Nevertheless, the use of pulsed laser diodes has emerged as a viable solution that, in addition to drastically reducing equipment investment, will facilitate the implementation of these tools in complex industrial environments, albeit with certain technical limitations. The integration of these excitation sources with interferometers points to a clear direction toward the future development of real-time applications for manufacturing process monitoring.

The third persistent challenge lies in image reconstruction through algorithms, which currently demand prohibitive computational costs and long processing times, or produce low-resolution images with the presence of artifacts. Overcoming these algorithmic barriers will be key to the development of robust in situ inspection systems capable of generating high-fidelity defect maps in a fraction of the current time. By resolving these mathematical limitations, photoacoustic technology will not only expand its own horizons but will also consolidate itself as an invaluable complement to traditional and current Non-Destructive Testing techniques.

6. Acknowledgment

JMDD acknowledges support from SECIHTI through the Doctoral Scholarship. LFEH and OMMC acknowledge support from SECIHTI (Secretaría de Ciencias, Humanidades, Tecnología e Innovación) through postdoctoral grants: Estancias Posdoctorales por México para la Formación y Consolidación de las y los Investigadores por México. FJGR acknowledges support from TecNM through the sabbatical stay AS-2-186/2025 and from PRODEP through the program Apoyos para el Fortalecimiento de Cuerpos Academicos MOO/3070/2025. This research was partially supported by SECIHTI (Grant No. CBF2023-2024-3038) and was also partially supported by DAIP-Universidad de Guanajuato: CIIC (Grant No. 401/2025).

Authorship acknowledgment

All authors contributed equally to the conception, development, and writing of this work. Each author participated in the research, analysis, and preparation of the manuscript, and all share equal responsibility for its content.

ISSN: 2594-1925

References

[1] B. Riveiro and M. Solla, Non-destructive techniques for the evaluation of structures and infrastructure, vol. 11. Boca Raton, FL, USA: CRC Press, 2016.
[2] S. K. Dwivedi, M. Vishwakarma, and A. Soni, "Advances and Researches on Non-Destructive Testing: A Review," Materials Today: Proceedings, vol. 5, no. 2, pt. 1, pp. 3690–3698, 2018, doi: 10.1016/j.matpr.2017.11.620.
[3] V. Vasagar, M. K. Hassan, A. M. Abdullah, et al., "Non-destructive techniques for corrosion detection: A review," Corrosion Engineering, Science and Technology: The International Journal of Corrosion Processes and Corrosion Control, vol. 59, no. 1, pp. 56–85, 2024, doi: 10.1177/1478422X241229621.
[4] C. Mandache, "Overview of non-destructive evaluation techniques for metal-based additive manufacturing," Materials Science and Technology, vol. 35, no. 9, pp. 1007–1015, 2019, doi: 10.1080/02670836.2019.1596370.
[5] J. García-Martín, J. Gómez-Gil, and E. Vázquez-Sánchez, "Non-Destructive Techniques Based on Eddy Current Testing," Sensors, vol. 11, no. 3, pp. 2525–2565, 2011, doi: 10.3390/s110302525.
[6] M. Gupta, M. A. Khan, R. Butola, and R. M. Singari, "Advances in applications of Non-Destructive Testing (NDT): A review," Advances in Materials and Processing Technologies, vol. 8, no. 2, pp. 2286–2307, 2022, doi: 10.1080/2374068X.2021.1909332.
[7] C. C. Roshan, C. Raghul, H. V. Ram, K. Suraj, and J. Solomon, "Non-destructive testing by liquid penetrant testing and ultrasonic testing—A review," Int. J. Adv. Res. Ideas Innov. Technol., vol. 5, no. 2, pp. 694–697, 2019.
[8] H. G. Tattersall, "The ultrasonic pulse-echo technique as applied to adhesion testing," Journal of Physics D: Applied Physics, vol. 6, no. 7, p. 819, May 1973, doi: 10.1088/0022-3727/6/7/305.
[9] S. A. Titov, R. G. Maev, and A. N. Bogachenkov, "Pulse-echo NDT of adhesively bonded joints in automotive assemblies," Ultrasonics, vol. 48, nos. 6–7, pp. 537–546, 2008, doi: 10.1016/j.ultras.2008.07.001.
[10] A. Lopez, R. Bacelar, I. Pires, T. G. Santos, J. P. Sousa, and L. Quintino, "Non-destructive testing application of radiography and ultrasound for wire and arc additive manufacturing," Additive Manufacturing, vol. 21, pp. 298–306, 2018, doi: 10.1016/j.addma.2018.03.020.
[11] P. A. Howell, Ed., Nondestructive Evaluation (NDE) Methods and Capabilities Handbook (NASA/TM–2020-220568/Volume I). NASA Langley Research Center, 2020.
[12] A. G. Bell, "On the production and reproduction of sound by light," American Journal of Science, vol. s3-20, no. 118, pp. 305–324, 1880.
[13] L. F. Derramadero-Domínguez, F. J. Escamilla-Herrera, O. M. García-Rodríguez, F. J. Medina-Cázares, F. J. Muñoz-Barbosa, and G. Gutiérrez-Juárez, "Laser-induced ultrasound: Consequences of Maxwell–Cattaneo–Vernotte 1D heat flux model," MRS Advances, 2025, doi: 10.1557/s43580-025-01128-8.
[14] E. Royer and E. Dieulesaint, "Analysis of thermal generation of Rayleigh waves," Journal of Applied Physics, vol. 56, no. 9, pp. 2507–2511, 1984, doi: 10.1063/1.334314.
[15] R. Zhang, X. Zhao, J. Li, D. Zhou, H. Guo, Z.-Y. Li, and F. Li, "Programmable photoacoustic patterning of microparticles in air," Nature Communications, vol. 15, no. 1, p. 3250, 2024, doi: 10.1038/s41467-024-47631-8.

ISSN: 2594-1925

[16] L. Xie, Y. Lian, F. Du, Y. Wang, and Z. Lu, "Optical methods of laser ultrasonic testing technology in the industrial and engineering applications: A review," Optics & Laser Technology, vol. 176, p. 110876, 2024, doi: 10.1016/j.optlastec.2024.110876.
[17] D. Ren, Y. Sun, J. Shi, and R. Chen, "A Review of Transparent Sensors for Photoacoustic Imaging Applications," Photonics, vol. 8, no. 8, p. 324, 2021, doi: 10.3390/photonics8080324.
[18] J. M. Escamilla-Herrera, L. F. Derramadero-Domínguez, O. M. Medina-Cázares, J. E. Alba-Rosales, F. J. García-Rodríguez, and G. Gutiérrez-Juárez, "On the dual-phase-lag thermal response in the pulsed photoacoustic effect: A theoretical and experimental 1D approach," Journal of Applied Physics, vol. 136, no. 17, p. 175105, 2024, doi: 10.1063/5.0226434.
[19] M. Xu and L. V. Wang, "Photoacoustic imaging in biomedicine," Review of Scientific Instruments, vol. 77, no. 4, p. 041101, Apr. 2006, doi: 10.1063/1.2195024.
[20] G. Ruiz-Veloz, R. I. Martínez-Ponce, R. Fernández-Ayala, R. Castro-Beltrán, L. Polo-Parada, B. Reyes-Ramírez, and G. Gutiérrez-Juárez, "Thermally corrected solutions of the one-dimensional wave equation for the laser-induced ultrasound," Journal of Applied Physics, vol. 130, no. 2, p. 025104, Jul. 2021, doi: 10.1063/5.0050895.
[21] R. Gao, Y. Liu, S. Qi, L. Song, J. Meng, and C. Liu, "Influence mechanism of the temporal duration of laser irradiation on photoacoustic technique: a review," Journal of Biomedical Optics, vol. 29, no. S1, pp. S11530–S11530, 2024, doi: 10.1117/1.JBO.29.S1.S11530.
[22] J. Krautkrämer and H. Krautkrämer, Ultrasonic Testing of Materials, 4th ed. Berlin: Springer-Verlag, 1990.
[23] M. Fang, X. Jing, S. Gao, J. Zhao, and T. Zhang, "Combining Windowed Enveloping and the Delay and Sum Algorithm for Photoacoustic Image Reconstruction," Applied Sciences, vol. 15, no. 9, p. 4877, 2025, doi: 10.3390/app15094877.
[24] B. D. Van Veen and K. M. Buckley, "Beamforming: A versatile approach to spatial filtering," IEEE ASSP Magazine, vol. 5, no. 2, pp. 4–24, 1988.
[25] A. Thomas, S. Paul, J. Mitra, and M. S. Singh, "Enhancement of Photoacoustic Signal Strength with Continuous Wave Optical Pre-Illumination: A Non-Invasive Technique," Sensors, vol. 21, no. 4, p. 1190, 2021, doi: 10.3390/s21041190.
[26] H. O. Durmuş, C. Birlikseven, B. Karaböce, and M. Seyitsoy, "Investigation of photoacoustic effect on different materials," in Proc. 2022 Medical Technologies Congress (TIPTEKNO), Oct. 2022, pp. 1–4, IEEE.
[27] Y.-M. Guo, Z. Liu, Y. Liang, X. Yin, and B. Ma, "Ppm-level photoacoustic oxygen gas sensor with a 3W red diode laser," Opt. Express, vol. 34, pp. 7895–7903, 2026.
[28] D. Vangi, M. S. Gulino, and A. Virga, "Optimal Rayleigh Waves Generation by Continuous Wave Modulated Laser," J. Phys.: Conf. Ser., vol. 1110, p. 012006, 2018, doi: 10.1088/1742-6596/1110/1/012006.
[29] D. Vangi, L. Banelli, and M.-S. Gulino, "Interference-based amplification for CW laser-induced photoacoustic signals," Ultrasonics, vol. 110, p. 106270, 2021, doi: 10.1016/j.ultras.2020.106270.
[30] X. Yan, S. Song, and H. Jin, "All-optical photoacoustic tomography via beam deflection," Journal of Physics D: Applied Physics, vol. 59, no. 3, p. 035401, 2026.
[31] V. T. Nguyen, C. Taboada, J. Delia, T. Vu, L. Menozzi, S. W. Cho, et al., "Dual-channel high-speed functional photoacoustic microscopy with ultra-wide field of view," Light: Science & Applications, vol. 15, no. 1, p. 91, 2026.

ISSN: 2594-1925

[32] M. Rojas-Romero, O. Medina-Cázares, F. J. García-Rodríguez, A. González-Vega, G. Martínez-Ponce, and G. Gutiérrez-Juárez, “Accurate internal cavities and kissing bond sizing in metal plates by using the time-of-flight of laser-induced ultrasound waves,” Applied Optics, vol. 63, no. 13, pp. 3641–3647, May 2024, doi: 10.1364/AO.519588.
[33] L. V. Wang and S. Hu, “Photoacoustic tomography: In vivo imaging from organelles to organs,” Science, vol. 335, no. 6075, pp. 1458–1462, 2012.
[34] J. Zheng, W. Dong, J. Sun, Q. Song, X. Jiang, S. Wang, S. Liu, and C. Tian, “TT-PADM: A Time-Driven Transformer Diffusion Model for Robust Sparse-View and Limited-View Photoacoustic Tomography,” BME Frontiers, vol. 7, p. 0237, 2026, doi: 10.34133/bmef.0237.
[35] A. M. Yu, X. Huang, S. Morais, J. H. Park, D. A. Zopf, S. J. Hollister, and S. Y. Emelianov, “Quantitative photoacoustic tomography of skin vasculature predicts subcutaneous implant exposure,” J. Biomed. Opt., vol. 31, no. 2, p. 026005, Feb. 2026, doi: 10.1117/1.JBO.31.2.026005.
[36] V. M. Moock, M. P. Colín-García, R. E. Camacho-López, O. E. Morales-Toledo, and A. Pérez-Pacheco, “Dual illumination and detection photoacoustic tomography of hollow metal cylinders,” Applied Sciences, vol. 15, p. 11967, 2025, doi: 10.3390/app152211967.
[37] Z. Chen, J. Zhang, C. Liu, C. Yang, and S. Chen, “Thermal Runaway in Lithium-Ion Batteries: A Review of Mechanisms, Prediction Approaches, and Mitigation Strategies,” Batteries, vol. 12, p. 88, 2026, doi: 10.3390/batteries12030088.
[38] M. Winter and R. J. Brodd, “What Are Batteries, Fuel Cells, and Supercapacitors?,” Chem. Rev., vol. 104, no. 10, pp. 4245–4270, Sep. 2004, doi: 10.1021/cr020730k.
[39] Y. Che, C. Duan, K. Yang, X. Di, X. Liu, C. Xiong, et al., “Cellulose-based separators in aqueous zinc-ion batteries: Mechanistic strategies for dendrite suppression and performance enhancement,” Carbohydrate Polymers, p. 124963, 2026, doi: 10.1016/j.carbpol.2026.124963.
[40] S. Jeong, C. Kim, V. S. Avvaru, G. Teeter, J. Ahn, G. Yang, and H. Kim, “Self-Healing Lithium Dendrites through Spontaneous Passivating Layer Formation for Stable Solid-State Lithium–Metal Batteries,” ACS Nano, 2026.
[41] H. Liu, Y. Zhao, J. Zhou, P. Li, S.-H. Bo, and S.-L. Chen, "Photoacoustic Imaging of Lithium Metal Batteries," ACS Applied Energy Materials, vol. 3, no. 2, pp. 1260–1264, Feb. 2020, doi: 10.1021/acsaem.9b01791.
[42] K. Nomura, S. Ishifuro, and S. Asai, “Study on Non-Contact Defect Detection Using the Laser Ultrasonic Method for Friction Stir-Welded Cu–Al Dissimilar Material Joints,” Applied Sciences, vol. 16, p. 688, 2026, doi: 10.3390/app16020688.
[43] C. Millon, A. Vanhoye, A. F. Obaton, and J. D. Penot, “Development of laser ultrasonics inspection for online monitoring of additive manufacturing,” Welding in the World, vol. 62, no. 3, pp. 653–661, 2018, doi: 10.1007/s40194-018-0570-7.
[44] G. Davis, R. Nagarajah, S. Palanisamy, R. A. R. Rashid, P. Rajagopal, and K. Balasubramaniam, “Laser ultrasonic inspection of additive manufactured components,” The International Journal of Advanced Manufacturing Technology, vol. 102, no. 5, pp. 2571–2579, 2019, doi: 10.1007/s00170-018-03257-9.
[45] Y. Jiang et al., “Quantitative Imaging Detection of Additive Manufactured Parts Using Laser Ultrasonic Testing,” IEEE Access, vol. 8, pp. 186071–186079, 2020, doi: 10.1109/ACCESS.2020.3030307.

ISSN: 2594-1925

[46] Z. Zhou, K. Zhang, J. Zhou, G. Sun, and J. Wang, "Application of laser ultrasonic technique for non-contact detection of structural surface-breaking cracks," Optics & Laser Technology, vol. 73, pp. 173–178, 2015, doi: 10.1016/j.optlastec.2015.04.026.
[47] Y.-K. An, B. Park, and H. Sohn, "Complete noncontact laser ultrasonic imaging for automated crack visualization in a plate," Smart Mater. Struct., vol. 22, no. 2, p. 025022, Jan. 2013, doi: 10.1088/0964-1726/22/2/025022.
[48] G. Zhang, S. Dong, Q. Xin, L. Guo, X. Wang, G. Xin, et al., "Transistor-level thermal management in wide and ultra-wide bandgap power semiconductor transistors: A review," International Journal of Thermal Sciences, vol. 219, p. 110200, 2026, doi: 10.1016/j.ijthermalsci.2026.110200.
[49] G. Galioto, G. Vitale, A. Sferlazza, G. Lullo, and G. C. Giaconia, "Wide and Ultrawide Bandgap Power Semiconductors: A Comprehensive System-Level Review," Electronics, vol. 15, p. 835, 2026, doi: 10.3390/electronics15040835.
[50] L. Wang, F. Yang, Y. Pei, et al., "Packaging and integration of silicon carbide power devices," Nature Reviews Electrical Engineering, vol. 3, pp. 157–172, 2026, doi: 10.1038/s44287-026-00263-0.
[51] P.-C. Chen, W.-C. Miao, T. Ahmed, et al., "Defect Inspection Techniques in SiC," Nanoscale Research Letters, vol. 17, p. 30, 2022, doi: 10.1186/s11671-022-03672-w.
[52] S.-H. Huang and Y.-C. Pan, "Automated visual inspection in the semiconductor industry: A survey," Computers in Industry, vol. 66, pp. 1–10, 2015, doi: 10.1016/j.compind.2014.10.006.
[53] Y. Yin, J. Xia, H. Nie, B. Yao, D. Sun, L. Ma, R. Li, Z. Li, and B. Zhang, "Numerical simulation analysis of laser ultrasonic detection of defects in silicon carbide," Crystals, vol. 15, no. 2, p. 125, 2025, doi: 10.3390/cryst15020125.
[54] K. Zhang, Z. Zhou, J. Zhou, and G. Sun, "Characteristics of laser ultrasound interaction with multi-layered dissimilar metals adhesive interface by numerical simulation," Appl. Surf. Sci., vol. 353, pp. 284–290, 2015.
[55] A. Alshaya, G. Alabduljabbar, and A. Alalwan, "Machine-learning-based real-time photoacoustic surface crack detection," Engineering Proceedings, vol. 56, no. 1, p. 92, 2023, doi: 10.3390/ASEC2023-15328.
[56] E. Dieussaert, R. Baets, H. Jans, et al., "Non-contact photoacoustic imaging with a silicon photonics-based Laser Doppler Vibrometer," Sci. Rep., vol. 14, no. 22953, 2024, doi: 10.1038/s41598-024-74266-y.
[57] A. Alifkalaila, Mitrayana, and R. Widyaningrum, "Photoacoustic imaging system based on diode laser and condenser microphone for characterization of dental anatomy," Int. J. Adv. Sci. Eng. Inf. Technol., vol. 11, no. 6, pp. 2363–2368, Dec. 2021, doi: 10.18517/ijaseit.11.6.12902.
[58] I. Huen, R. Zhang, R. Bi, X. Li, M. Moothanchery, and M. Olivo, "An investigation of signal preprocessing for photoacoustic tomography," Sensors, vol. 23, no. 1, p. 510, 2023, doi: 10.3390/s23010510.
[59] Y. Sun and H. Jiang, "Enhancing finite element-based photoacoustic tomography by localized reconstruction method," Photonics, vol. 9, no. 5, p. 337, 2022, doi: 10.3390/photonics9050337.
[60] P. Hu, L. Ai, Z. Qiu, J. Zuo, S. Liu, Y. Liu, Z. Peng, and C. Song, "Laser ultrasonic nondestructive testing on metal additive manufacturing components," Chinese Journal of Lasers, vol. 49, no. 14, p. 1402803, 2022, doi: 10.3788/CJL202249.1402803.
[61] R. Burger, D. Wu, and C. U. Grosse, "Non-destructive evaluation and defect characterization of ceramic matrix composites using laser ultrasonics," in Proc. 9th Int. Congr. Ultrasonics (ICU), Paderborn, Germany, Sept. 21–25, 2025, pp. 263–266, doi: 10.5162/Ultrasonic2025/D3-a5.

ISSN: 2594-1925

[62] D. Vangi, M. S. Gulino, N. Montinaro, C. Mineo, D. Cerniglia, and G. Epasto, "On the use of two emerging laser-based flaw-detection techniques – considerations and practicalities," Optics and Lasers in Engineering, vol. 165, p. 107551, 2023, doi: 10.1016/j.optlaseng.2023.107551.

ISSN: 2594-1925